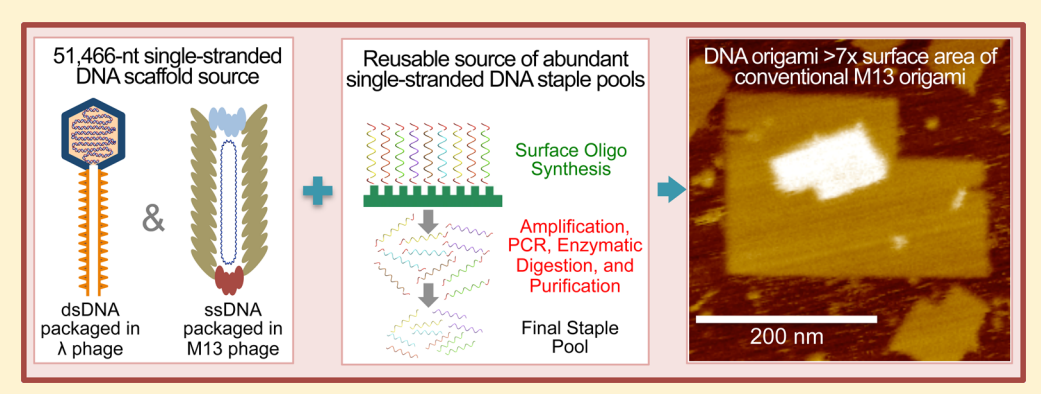


Toward Larger DNA Origami

Alexandria N. Marchi,[†] Ishtiaq Saaem,^{†,||} Briana N. Vogen,[‡] Stanley Brown,[§] and Thomas H. LaBean*,^{†,‡}

Supporting Information



ABSTRACT: Structural DNA nanotechnology, and specifically scaffolded DNA origami, is rapidly developing as a versatile method for bottom-up fabrication of novel nanometer-scale materials and devices. However, lengths of conventional singlestranded scaffolds, for example, 7,249-nucleotide circular genomic DNA from the M13mp18 phage, limit the scales of these uniquely addressable structures. Additionally, increasing DNA origami size generates the cost burden of increased staple-strand synthesis. We addressed this 2-fold problem by developing the following methods: (1) production of the largest to-date biologically derived single-stranded scaffold using a $\lambda/M13$ hybrid virus to produce a 51 466-nucleotide DNA in a circular, singlestranded form and (2) inexpensive DNA synthesis via an inkjet-printing process on a chip embossed with functionalized micropillars made from cyclic olefin copolymer. We have experimentally demonstrated very efficient assembly of a 51kilobasepair origami from the $\lambda/M13$ hybrid scaffold folded by chip-derived staple strands. In addition, we have demonstrated two-dimensional, asymmetric origami sheets with controlled global curvature such that they land on a substrate in predictable orientations that have been verified by atomic force microscopy.

KEYWORDS: Nanotechnology, structural DNA nanotechnology, DNA origami, lambda DNA, on-chip DNA synthesis, hybrid bacteriophage

he ultimate goal of nanofabrication is to build functional, atomically precise materials. Retention of atomic-scale precision of matter as length-scales increase is becoming available through bottom-up fabrication. Biological systems have inspired molecular self-assembly techniques for harnessing physicochemical forces to specifically position atoms within intricate assemblies. Of the biomolecules tested as molecular building materials, nucleic acids have gained special attention. Specifically, deoxyribonucleic acid (DNA) is a stable molecule with predictable and programmable intermolecular interactions. These properties are exploited in the revolutionary structural DNA nanotechnology method known as scaffolded DNA origami.² Synthetic oligonucleotides (staple strands) are designed to fold a long, single-stranded viral DNA (scaffold strand), conventionally isolated from M13 bacteriophage into discrete shapes with full addressability. Origami structures provide functional surfaces for the specific arrangement of inorganic and organic materials with precision down to the single-digit nanometer scale.3-13

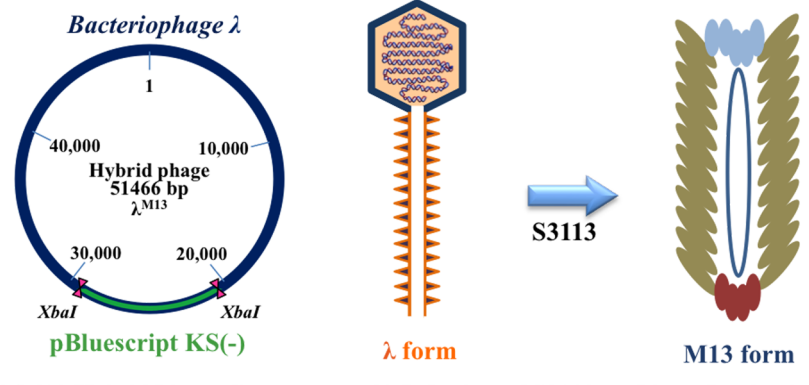
An objective of the DNA nanotechnology community is increasing the available surface area or mass of origami and therefore the number of unique addresses at which nanometerscale materials can be organized (e.g., bigger breadboards). Recent approaches to scale up origami include connecting preformed structures, 14-19 using a biologically derived double-stranded DNA (dsDNA) scaffold, 20-22 or enzymatically producing a single-stranded DNA (ssDNA) scaffold.²³ These strategies suffer from complicated multistep anneals, low yield of final product, and/or complex mixtures of misassembled contaminants. In general, forming DNA origami from a singlestranded scaffold is faster and cleaner because sequence

Received: July 11, 2014 Revised: August 26, 2014 Published: September 1, 2014

[†]Biomedical Engineering Department, Duke University, Durham, North Carolina 27708, United States

^{*}Materials Science and Engineering Department, North Carolina State University, Raleigh, North Carolina 27606, United States

[§]Department of Biology and Niels Bohr Institute, University of Copenhagen, Copenhagen N, Denmark-2200



a) λ /M13 Hybrid Phage Genome

b) Infection of S3113: ss Phage Production

Figure 1. Schematic for production of single-stranded $\lambda/\text{M13}$ hybrid phage. (a) The pBluescript phagemid was cloned into λ at the XbaI restriction site to produce λ^{M13} . The bacteriophage λ form of λ^{M13} is a virus particle containing dsDNA. (b) *E. coli* strain S3113, harboring the helper plasmid pSB4423, is infected with λ^{M13} . S3113 diverts growth of λ^{M13} from its dsDNA λ form to its ssDNA M13 form. The pSB4423 helper phage provides for production of M13 coat proteins but is itself defective for packaging.

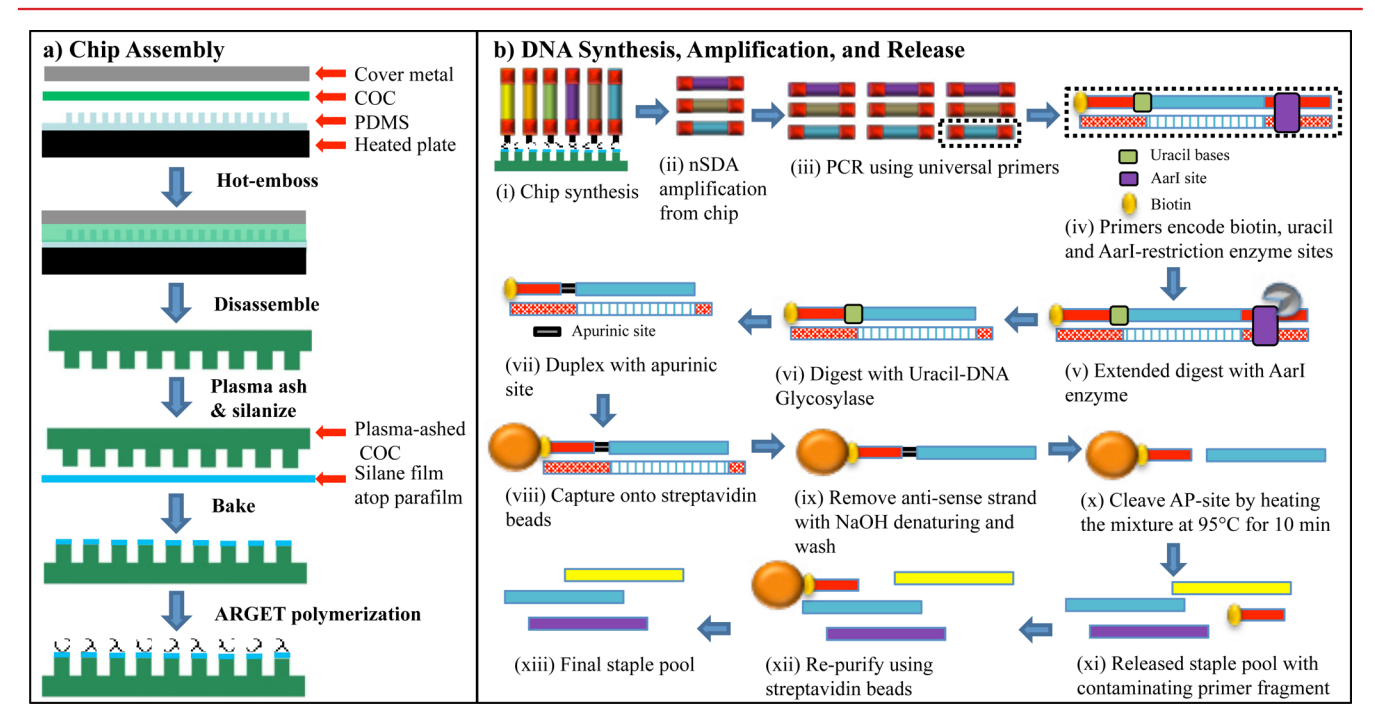


Figure 2. Schematics for chip fabrication and staple pool liberation. (a) Micropillars were hot-embossed on COC chip substrates. (b) Staple strands were individually synthesized on pillars and amplified off the chip surface by nSDA. Oligonucleotides were then amplified via PCR and released as single-stranded DNA.

complementarity does not interfere with staple interrogation of the scaffold, while origami formed from double-stranded scaffolds requires chemical denaturants.

To increase the size of origami structures, an increase in the scaffold size as well as the number of staple strands used to fold the scaffold are needed. While prices of synthesized oligonucleotides have decreased significantly over the past several years, DNA origami requires a very large number of unique strands. Folding conventional origami requires over 200 distinct DNA staple strands each around 32 bases long, which is over 7000 synthesized bases. Custom synthesized DNA oligos cost \$0.35 per base at a 25 nmole synthesis scale with the lowest level of purification applied. For 200 staples, individual synthesis would cost over \$2000 for the staples necessary for testing a single origami design. This substantial cost retards rapid design and testing of various DNA origami structures.

Here we describe two methods that overcome some of the major challenges for future progress of the DNA origami field: (1) biological production of a 51 466-nucleotide single-strand of DNA (51-knt) derived from a $\lambda/M13$ hybrid phage and (2) staple synthesis, amplification, and release in high yield from a uniquely formulated chip substrate at a cost of less than \$0.001/ bp. 25 This single-stranded scaffold folds into large, well-formed origami structures that rapidly assemble with high yield as observed via atomic force microscopy (AFM) imaging. The simple notched rectangle (NR) shape allows AFM imaging to determine which side of the origami is facing up when adsorbed onto mica surfaces. Manipulating the DNA helical twist by adjusting the spacings between crossovers results in structures that exhibit global curvature and twisting.²⁶ We have taken advantage of this by creating three different NR origami designs with three different staple strand sets. Notched rectangles were

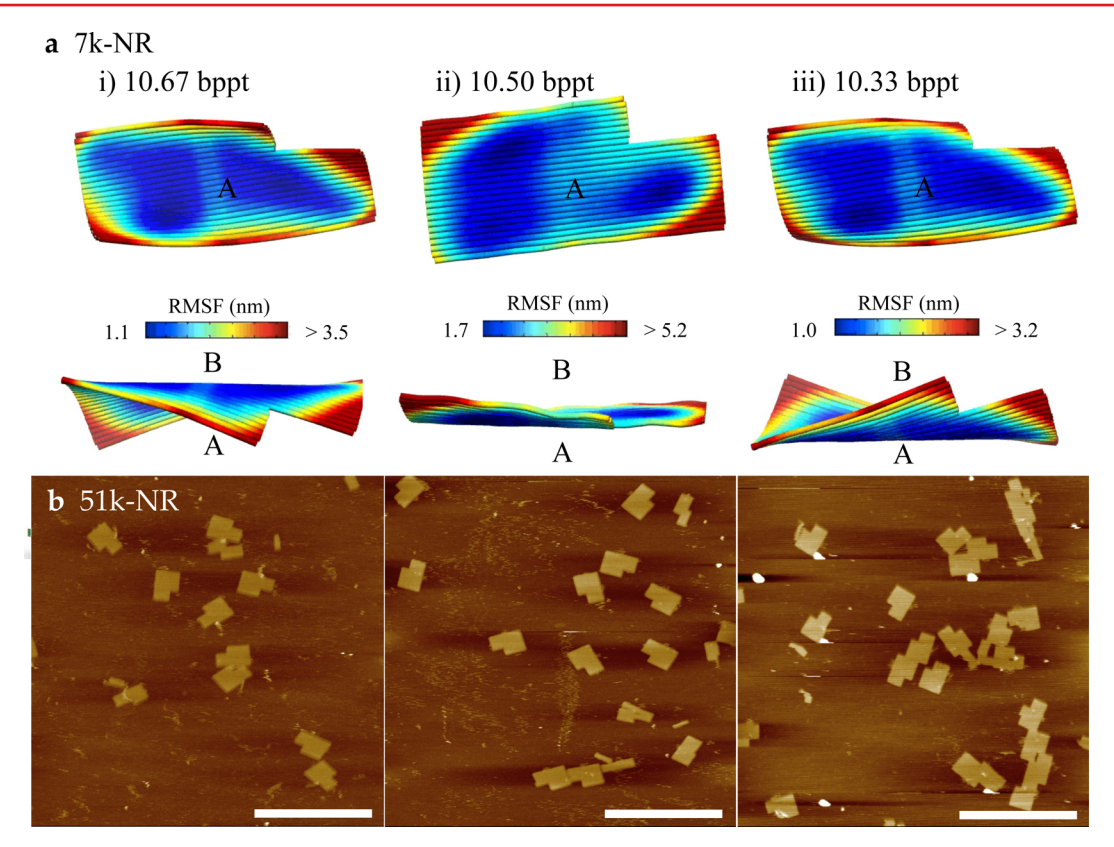


Figure 3. Models of DNA origami designs (7k-NR) and corresponding AFM images (51k-NR). (a) CanDo prediction of the average solution structure of the notched rectangle (NR) DNA origami structures designed to the scale of the M13 scaffold. The coloration indicates the flexibility of the predicted structures given as root-mean-square fluctuations (RMSF) in nanometers. "A" and "B" define the faces of the origami. (b) Example AFM images of the various 51-kbp notched rectangles with the number of basepairs per helical turn (bppt) indicated above. Scale bars are 1 μ m.

designed with varied numbers of basepairs between crossovers such that they were predicted to be either flat or have global curvature in solution. We hypothesize that NRs with different curvatures will land on charged surfaces with a bias toward landing on the face that presents the most charged surface area when approaching the surface (i.e., the convex side of the sheet). Our three designs allowed us to demonstrate this bias by analyzing the asymmetric structures by AFM.

Results. Single-Stranded Scaffold Development. In this work, we have facilitated the high-yield assembly of larger DNA origami by developing a method for biological production of a 51 466-nt ssDNA scaffold strand. To produce the 51-knt ssDNA scaffold, we prepared a hybrid bacteriophage where we controlled its mode of replication by propagation on one of two host bacteria. The 51-knt ssDNA scaffold strand was produced via two sequential infections. Initially, M13 phagemid DNA (pBluescript KS(-), Strategene) was cloned into doublestranded λ DNA at the XbaI restriction endonuclease site (both λ and pBluescript KS(-) contain exactly one XbaI cutting site) (Figure 1a). This hybrid phage now harbors three origins of replication: (1) a double-stranded origin from λ , (2) a doublestranded colEI origin from pBluescript KS(-), and (3) a singlestranded M13 origin from pBluescript KS(-) (see Supporting Information Table S1). This $\lambda/M13$ hybrid phage $(\lambda^{\overline{M13}})$ was maintained as a temperature-inducible prophage in the genome of Escherichia coli. A second strain of E. coli, S3113, was infected with the released λ^{M13} viruses. S3113 diverts development of λ^{M13} to produce a ssDNA, M13 form of the bacteriophage (Figure 1b). The released ssDNA phage were purified by PEG fractionation and CsCl gradient centrifugation. The ssDNA

was extracted from the purified phage by phenol/chloroform extraction, and ethanol precipitation. The purified 51kb ssDNA was homogeneous in size as determined by agarose gel electrophoresis (see Supporting Information Figure S1).

Chip Formulation and Staple-Strand Synthesis. The cost for production of numerous short oligos (staple strands), necessary for scaffolded DNA origami formation, discourages the use of origami to solve interdisciplinary problems. To combat this obstructive cost, our large structures were annealed with pools of chip-derived staples that cost less than \$0.001/bp.²⁵ This significantly reduced the expense of origami production when surveying numerous designs. Phosphoramidite chemistry was used for DNA staple set synthesis with the reagents being delivered to a chip substrate, as previously described. ²¹ All staple sequences were appended with a universal primer pair with one primer encoding an AarI restriction enzyme site. Complementary versions of these sequences were further appended with a 25base adaptor at the 3' end, which provided a nicking site and anchored the oligo to the chip surface. Micropillars, made from cyclic olefin copolymer (COC), were grafted with poly-2hydroxyethyl methacrylate (polyHEMA) using activators regenerated by electron transfer atom transfer radical polymerization (ARGET ATRP) (Figure 2a). Staples were synthesized on grafted substrates and amplified from the surface-bound template (Figure 2b). With this unique chip development and amplification strategy, we were able to recover greater than one microgram of DNA from a single chip.

DNA Origami Designs. DNA origami structures are assembled with staple strands that bind to different parts of the scaffold strand creating uniformly spaced crossovers. The

number of basepairs between each crossover determines the position in space of neighboring DNA helices. Conventional two-dimensional DNA origami structures are comprised of neighboring helices held together by crossovers that are 32 basepairs apart. The intention was to produce a planar structure with 32 basepairs per three helical turns of the DNA. However, this pattern requires that the helical twist of a DNA molecule be 10.67 basepairs per turn (bppt). Recent structural analysis by small-angle X-ray scattering shows solution conformations of double-stranded B-DNA with 10.5 basepairs per helical turn.²⁷ Forcing crossovers every 32 basepairs under-twists the DNA helices compared with the native conformation. To compensate for this underwinding, the global origami structure is intrinsically curved. We can control which face of the origami is convex or concave by varying the number of basepairs between crossovers, that is, 32 basepairs between crossovers assumes 10.67 bppt, producing a curved origami where side A is on the concave side versus 31 basepairs between crossovers assumes 10.33 bppt, producing a curved origami where side A is on the convex side. Additionally, alternating between 32 and 31 basepairs between crossovers creates a relatively flat origami by balancing the overand under-twisted helices, corresponding to the natural 10.50 basepairs per turn.

With the rising interest in DNA origami, software has been developed to simplify the design of two- and three-dimensional structures following the origami architectural constraints.²⁸⁻³⁰ One such program, caDNAno, 30 was used to design the notched rectangle origami made from the 51-knt scaffold (51k-NR) with three varied pitches: 10.33, 10.50, and 10.67 bppt. The complementary modeling program, CanDo,³¹ is a web serverbased computational resource that uses finite element modeling to predict the conformational ensemble of origami structures in solution based on mechanical properties of DNA and design criteria of the modeled object. Because our 51-kpb origami exceeded the input size limit of CanDo, we modeled scaled-down versions (reduced in size to the 7249-nt ssM13mp18 scaffold, 7k-NR) of our asymmetric 51k-NR with 10.67, 10.50, and 10.33 basepairs per turn. Subsequently, these three designs from caDNAno were modeled by CanDo for solution structure prediction. The results showed deformed sheets that curve in the dimension perpendicular to the helical axes (Figure 3a). These models were then tested experimentally by examining the orientation of structures as imaged by AFM (Figure 3b).

The three-dimensional conformation of notched rectangles in solution was inferred by examining structure orientation on a surface by AFM. Samples were prepared by pipetting a suspension of origami onto freshly cleaved mica. Electrostatic forces between the negatively charged sugar-phosphate backbone of DNA and the positively charged Mg²⁺/mica surface cause the origami to flatten out upon contact with the surface. A curved notched rectangle approaching the mica surface with its convex face projects greater surface area toward the mica, which is directly related to the amount of electrostatic force drawing the origami to the surface. Therefore, collecting statistics on which face adheres to the mica surface most frequently can validate our predictions of the curvature of the origami. Designs with an average pitch of 10.33, 10.50, and 10.67 bppt were assembled with the 51 466-nt $\lambda/M13$ hybrid scaffold. Multiple AFM images were taken of each sample (see Supporting Information Note 5) and used to measure the distribution of origami orientations. Data summarized in Figure 4 corroborates the CanDo predictions for curvature, that is, in each case the convex face more frequently associates with the substrate.

Orientation of Origami from AFM

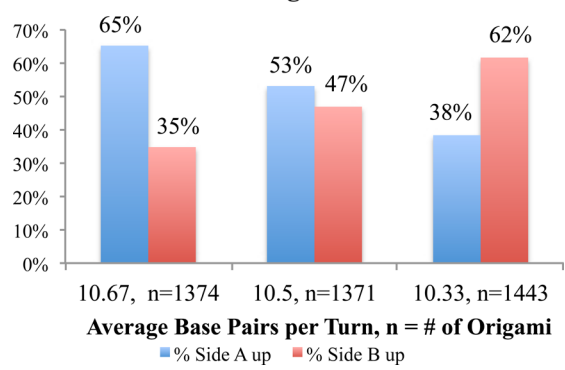


Figure 4. Percentages of origami structures facing "up" or "down" on AFM images. The positioning of the origami structures on the mica is specified by the inherent curvature due to over/under winding the DNA helices.

Optimizing DNA Origami Formation. Traditional thermal anneals of two-dimensional origami folding the single-stranded M13 scaffold are performed by mixing ssM13 with a molar excess of staples in the presence of buffer and magnesium ions. This solution is then heated to temperatures up to 95 °C, held for up to 10 min, and cooled to 20 °C in as quickly as an hour. After attempting thermal and chemically enhanced anneals, we found that the highest yield (as visualized by AFM) of 51k-NRs was produced with a quick, moderate temperature anneal (65 °C for 3 min, cooled to 20 $^{\circ}$ C at a rate of 1 $^{\circ}$ C/min). We reason that this lower incubation temperature was necessary due to the sensitivity to breakage of the 51-knt ssDNA scaffold. Heating the 51-knt scaffold to high temperatures led to degradation. Care was taken when pipetting by using large bore pipet tips to minimize shear forces. Similarly shaped NR origami were designed and annealed using the 7,249-nt single-stranded M13mp18 scaffold strand. AFM images of a mixture of similar NRs designed to have an average 10.50 bppt are shown in Figure 5 to illustrate the difference in scale. Fully intact notched rectangle origami was the predominant form observed by AFM. Our 51-kbp origami provides seven times the surface area of origami made from the traditional ssM13 scaffold and pushes the mass of fully addressable molecular assemblies to 14 times the size of the ribosome, at 34 megadaltons this may be the largest human-made, monodisperse, supramolecular assembly, to date.²

Discussion. To increase the achievable size of scaffolded DNA origami while maintaining the high product quality observed for conventional origami, a larger single-stranded DNA scaffold was prepared. Folding a single-stranded scaffold is less challenging than a double-stranded scaffold because competition between long complementary strands is eliminated, thus chemical denaturing agents are not necessary. Our colleagues have attempted to fold double-stranded DNA from the λ bacteriophage (48 502-nt) into a DNA origami structure.³² Their yields of structure formation are very low, which the authors attribute to the long, self-complementary doublestranded scaffold. Because folding a double-stranded scaffold into an origami structure in high yield seems to be limited by the length of the scaffold, we reasoned that the next logical approach was to increase the length of the single-stranded scaffold strand. As mentioned above, one methodology to produce singlestranded DNA is via long-range PCR amplification for the production of a 26-knt single-stranded DNA fragment, which is folded into a rectangle origami using 800 staple strands.²³ The

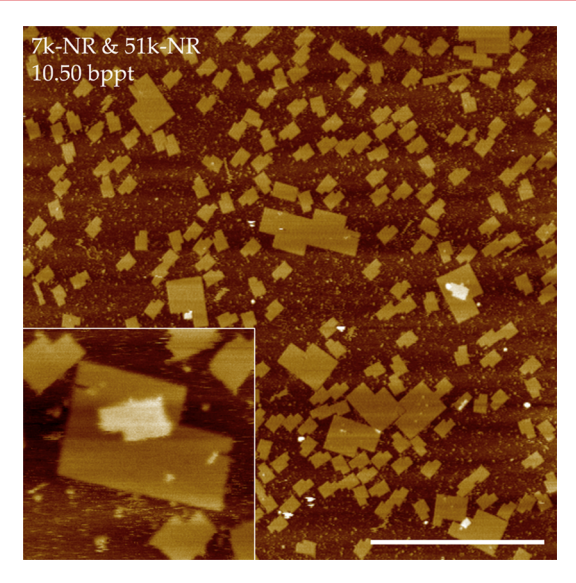


Figure 5. The 51-knt compared to ssM13 origami. The AFM image of a mixture of similar notched rectangles formed with ssM13mp18 and 51-knt scaffolds displays the advantage in scale (over 7 times the surface area) that the 51-knt scaffold offers over the conventional ssM13mp18 scaffold. Both notched rectangles were designed with 10.50 average basepairs per turn (bppt). Scale bar is 1 μ m. Inset is 400 nm square.

authors state that their poor efficiency of formation (as determined by AFM) could have been due to single-stranded DNA fragmentation, nonoptimized annealing conditions, and/or tip perturbation during AFM scanning. Instead, we exploited pathways of phage morphogenesis to develop a large single-stranded scaffold.

Few biological systems produce large, single-stranded DNA naturally. Therefore, we have used recombinant DNA techniques and molecular cloning in phagemid genetic engineering systems to develop our large single-stranded DNA scaffold. M13 is a single-stranded DNA bacteriophage. Because large derivatives of M13 are unstable during extensive propagation, we sought to reduce the number of generations our large scaffold was propagated as an M13 phage. We prepared a hybrid phage bearing components (including replication origins and repressors) from both phages λ and M13. Therefore, this hybrid phage could be propagated either as phage λ or phage M13. The form produced by the hybrid phage was determined by infecting one of two host bacteria such that both origins of replication could be regulated separately. Thus, single-stranded phage could be produced where only the final generation was propagated as M13.

The notched rectangle shape allowed us to distinguish between each face of the origami sheets after they had landed on a surface. Modifying the shape of the origami provided its asymmetric handedness without imposing another bulky item (e.g., a hairpin, conjugated moiety, or appended protein), which could have influenced the landing of the origami on the mica surface prior to AFM analysis. Presumably, the convex side of the origami would have a higher probability of landing and binding to the mica due to the increase in density of electrostatic interactions between the mica surface, divalent salt (Mg²⁺), and the negatively charged sugar—phosphate backbone of DNA. Folding and AFM imaging of the three designs discussed above under identical conditions showed the expected disproportionality of landing, correlating well with the predicted solution curvature results from the CanDo models. Also, because all three

designs produced well-formed structures, we were able to conclude that origami formed from the 51-knt $\lambda/\text{M13}$ hybrid DNA scaffold are flexible enough to bind tightly to mica surfaces without AFM tip perturbation.

The development of new origami designs is limited by the high costs of synthesizing hundreds of oligonucleotide staple strands. Development of methods for high-throughput synthesis of specific mixtures of high-quality oligos allows for more ambitious studies of the formation of DNA-based nanostructured materials. As promising substrates for solid-phase oligonucleotide synthesis, our new polymeric micropillar arrays are also amenable to high-throughput and low-cost industrial manufacturing. These methods involving embossing or injection-molding techniques require a much lower investment in capital equipment than processes utilizing photolithography. In our hands, synthesis substrates produced by embossing had lower variation from operator to operator than did our earlier deposited silica arrays.²² Additionally, the physical micropillars enabled easier optical alignment to the substrate on our home-built platform. Folding our 51k-NR origami required over 1600 distinct DNA staple strands, each around 32 bases long, over 51 200 synthesized bases in total. For 1600 staples, conventional custom DNA synthesis would currently cost over \$7000 in order to test a single origami design. With the method described here we reduce the cost of this staple pool by more than an order of magnitude.

Scaffolded DNA origami holds immense potential for programed self-assembly of objects, devices, and materials with nanometer-scale feature resolution; its ability to position distinct and diverse objects with single-digit nanometer precision is unmatched by any other method. Its popularity has spurred rapid progress in advancing the technique toward a functional material, overcoming some of the challenges for extending DNA origami into real-life applications. Notable publications increase yields of formation for three-dimensional structures,³³ use rate-zonal centrifugation for high-throughput purification,³⁴ and probe the structure of assemblies by electron microscopy.³⁵ However, these advances and others are most appropriately applied to conventional origami formation, specifically they work best with a single-stranded scaffold. While many anticipated hurdles for moving DNA origami toward commercial uses continue to be overcome, obtaining high assembly yields appears to require a single-stranded DNA scaffold.

Conclusion. For the DNA origami technique to establish itself as a useful strategy for various nanotechnology applications, the available length-scale must be increased and procedures for formation must be rapid and simple. Here we have described a method to produce a 51 466-nt single-stranded $\lambda/M13$ hybrid DNA scaffold. We validated its stability by folding the scaffold using chip-derived staple strands into multiple origami structures with increased scale and improved performance compared to previous reports of large origami structures. We also implemented a method to decrease the cost of origami production by improving the chip synthesis platform by employing embossed micropillar arrays, which reduced chip-tochip variability. Additionally, our secondary PCR process with template produced by on-chip nSDA has allowed significant material yield (>1 μ g), thereby allowing for many experimental trials of the design. Our approach toward reliable large-scale, high-yield, and low production cost of DNA origami structures in a simple one-pot anneal are marked advances toward structural DNA nanotechnology as a multifunctional tool for many potential applications.

Materials and Methods. Strains. pSB4423: HindIII - Sall fragment of pACYC184⁴⁰ was replaced with M13 from geneII through geneIV by PCR amplification of M13+ with 5′-TTTAACGCGaagcttAACAAAATATTAACGTTTACAA-3′ and 5′- GGAGgtcgacGTTACAGGGCGCGTAC-TATGGTTGCT-3′ (restriction recognition sites in lower case). Plasmid pSB4423 confers chloramphenicol-resistance.

Production of λ Form of λ^{M13} . The λ form of λ^{M13} was produced by temperature induction of the prophage in S3069, a lysogen of HO480 (Table 1). HO480 was used to prevent the

Table 1

strain	genotype	source
λ	bacteriophage λ	T. Silhavy
$\lambda^{ ext{M13}}$	λcI857 XbaI::pBluescript KS-	this study
HO480	F- polA1(Am) lysA	38
S1754	F- lacI ^q metA endA hsdR17 supE44 thi1 relA1 gyrA96	39
S3069	$HO480(\lambda^{M13})$	this study
S3113	$S1754(\lambda^{+}) pSB4423$	this study

ColE1 origin of replication in λ^{M13} from interfering with λ growth. Single colonies of S3069 were revived on YT agar at 30 °C. Presence of the prophage was detected as colonies able to grow at 30 °C but not 42 °C. Operationally, this test is performed by inoculating 4 mL YT broth with a single colony of S3069 and with the same inoculating loop, inoculating two plates; the first one to be inoculated was incubated at 42 °C and the second one at 30 °C. The liquid culture was incubated with aeration overnight at 30 °C. The next day, only temperature-sensitive cultures were used. An overnight culture was diluted into 100 mL of 2xYT supplemented with 10 mM potassium phosphate pH 7.5 and 20 mM MgSO₄. The culture was incubated with vigorous shaking. After an hour or so, clearing became apparent. Lysis was verified by removing a small sample and adding a drop of CHCl₃. When clearing was apparent, a few drops of CHCl₃ were added and shaking continued another 10 to 15 min. The lysed culture was clarified at 5000g, 10 min, 4 °C. The supernatant was decanted and filtered through sterile 0.45 µm filters into a sterile bottle. Filtered lysates were stored at 4 °C. The concentration of viable phage was determined after serial dilution with TMG (10 mM Tris-HCl pH 7.6, 5 mM MgCl₂, 0.1 mg/mL gelatin, autoclave) and titered by soft-agar overlay on HO480. The concentration of viable phage was recorded as plaque-forming units per mL of lysate (PFU/mL).

Production of M13 form of λ^{M13} . Conversion of the hybrid phage from its λ form to its M13 form was mediated by the use of an alternative host. Attempts to convert forms using the M13KO7³⁶ or M13-VCS (Stratagene) helper phages failed to divert packaging from the helper phage to the hybrid phage. To produce the M13 form of λ^{M13} we prepared a helper plasmid that lacked any single-stranded packaging sites, pSB4423. Infection of strain S3113 with the λ form of λ^{M13} diverts replication from the λ form to the M13 form. Moreover, the M13 form is unable to reinfect S3113 because S3113 lacks the surface receptor for infection by M13 phages.

A culture of S3113 was established at 30 °C in YT broth supplemented with 20 μ g/mL chloramphenicol, 10 mM MgSO₄, and 0.2% maltose. While in early- to mid log phase the culture was infected with λ S3069 at a multiplicity of infection <1. Incubation was continued 1 h to express ampicillin-resistance and infected culture diluted 10–20-fold into 2xYT supplemented with 5 mM each HEPES and sodium HEPES, 20 μ g/mL

chloramphenicol, 200 $\mu g/mL$ ampicillin and incubated with aeration overnight at 30 $^{\circ}C$.

Purification of Single-Stranded λ S3069. The outgrown infected culture was made 10 mM sodium-EDTA and clarified at 6000g, 15 min at 4 °C. Phage was purified by PEG precipitation and CsCl centrifugation as described by Yamamoto et al. 1970, except the CsCl gradient step was replaced by isopycnic centrifugation.³⁷ The clarified supernatant was decanted into a graduated cylinder and 1/4 volume of 10% w/ v PEG8000, 2.5 M NaCl was added. The suspension was mixed and incubated on ice for 4 h. The PEG-solvent-particle phase containing the M13 phage was recovered by centrifugation at 6000g, 20 min at 4 °C. The supernatant was discarded and the "pellet" resuspended with a few milliliters of 20 mM Tris-HCl pH 8, 5 mM EDTA, 0.5 M NaCl, 2% w/v PEG8000, and transferred to eppendorf tubes. The resuspended pellet was collected at 5000g, 5 min, 4 °C. The supernatant was discarded and the residual liquid transferred to the bottom of the centrifuge tube by brief centrifugation and removed by aspiration and discarded. The pellet was overlaid with TE to 1% of the original culture volume and incubated at 4 °C overnight. The resuspended material was dialyzed against 2xTE for 5 h and clarified at 10 000g, 5 min, 4 °C. Cesium chloride was added at 0.45 g per mL of supernatant and centrifuged with an SW41 rotor at 25 000 rpm, 22 h, 10 °C. The opalescent band was withdrawn and dialyzed versus two changes of 50 volumes of 2xTE, 0.1 M NaCl. The phage were deproteinized with phenol/chloroform, 3:1 and the residual phenol removed by extraction with chloroform. The DNA was recovered by precipitation with ethanol.

Staple Strand Synthesis Reagents. The materials and methods involving the inkjet printer and oligonucleotide synthesis have been reported previously. The 3-(trimethoxysilypropyl)-2-bromo-2-methylpropionate was purchased from Gelest. 2-Hydroxyethyl methacrylate (HEMA) and all other chemicals were purchased either from Sigma-Aldrich or VWR. Enzymes were from New England Biolabs.

Soft Mold Fabrication. Two processes were exploited to fabricate a PDMS master mold, which was used in embossing. Single-crystal 4-in. silicon (100) wafers were used as the substrate material in this experiment. Before the resist was dispensed, the substrates were cleaned using the RCA cleaning method (NH₄OH/H₂O₂/H₂O, 70 °C) and dehydrated. After cleaning, the silicon wafers were coated with commercially available SU-8 100 using a Headway spin coater (Garland, TX). Samples were prebaked at 65 °C and then 95 °C on two hot plates; baking time varied depending on resist thicknesses. Exposure was carried out in a Karl Suss MJB3 contact aligner using a broadband mercury lamp (illumination at 365 nm with 9.2 mW cm $^{-2}$). Post exposure bake (PEB) was carried out at 65 °C and then at 95 °C. Samples were developed in SU-8 developer and then blown dry under nitrogen flow.

The SU-8 resist patterns were transferred to an embossing master by casting PDMS on the positive structure. The Sylguard 184 silicone elastomer was thoroughly mixed with the curing agent in a weight proportion of 10:1. The mixture was degassed in a vacuum oven at room temperature for 30 min to remove air bubbles. The polymer mixture was poured over the SU-8 patterned masters and cured for 10 min at 90 $^{\circ}\mathrm{C}$ on a leveled hot plate. The assembly was cooled down to room temperature after the structures were polymerized and solidified. The polymer was carefully peeled off from the masters.

Hot Embossing. All hot embossing was carried out on a hydraulic hot presser (Carver, Wabash, WI). The parameters of

molding processes including molding temperatures, molding time, and pressures are discussed in Supporting Information Note 2. To achieve equal size and thickness of each embossed device, the entire embossing assembly was confined by a 4 in. round steel spacer with a 3 in. center hole. The height of the spacer is equal to the sum of the PDMS thickness and the designated COC device thickness. During embossing, the PDMS master was placed within the spacer hole with its patterned surface facing up. It was then covered with COC. A piece of metal with a mold of the same size was put on top of COC and its polished surface was face down. The entire stack was sat on a long piece of aluminum plate, which was used to transfer the assembly in and out of the presser. The two platens of the presser were preheated to the desired temperature, and embossing load was transferred inside. After certain amount of heating time, pressure was applied and the system was cooled down to the established demolding temperature. Master and substrate were then manually separated.

Synthesis Substrate Design. Synthesis was performed atop COC slides either deposited with silica thin-film spots or embossed with pillars functionalized with polyHEMA. For COC substrates with silica microarrays, methods were performed as described elsewhere. 21,42 For COC substrates with embossed pillars, embossed chips were plasma ashed for 10 min at 100 W and then incubated overnight in anhydrous toluene solution containing 18 µM 3-(trimethoxysilypropyl)-2-bromo-2-methylpropionate. HEMA (Sigma-Aldrich) was purified using a prepacked hydroquinone inhibitor remover column. The polymerization reaction was carried out in water and methanol (1:1 v/v) containing 0.6 M HEMA. Cu(II)Br (0.232 mg) was added to the solvent mixture along with PMDETA (ligand) (19.6 μ L). The polymerization reaction was initiated by the addition of ascorbic acid (3.5 mg) as the reducing agent, which activates the catalyst. The polymerization reaction was carried out for 6 min. Subsequent brushes were characterized by ellipsometry.

Staple Complement Synthesis. Synthesis was performed on either silica or polyHEMA functionalized COC substrates. In situ synthesis of DNA microarrays utilized standard phosphoramidite chemistry with a custom-built piezoelectric inkjet platform and subsequent nicking-strand displacement amplification (nSDA) was performed as reported previously.^{21,42}

PCR Amplification and Single-Stranded DNA Release. From the above pool (seed eluate), 0.5 ng was amplified using universal primers in a 100 µL polymerase chain reaction. One primer contains a Uracil base at the 3' end and a 5' dual-biotin. The other primer encodes an AarI restriction enzyme site. The reaction contained 1 µM of each primer, 0.25 mM dNTPs, and $0.1\,\mu\mathrm{L}\,(2\,\mathrm{U})$ of Phusion DNA polymerase. The following cycling protocol was applied: 98 °C for 30 s; 35 cycles of 98 °C for 10 s; 60 °C for 10 s; 72 °C for 10 s; 72 °C for 60 s and then hold at 4 °C. PCR reactions are then purified using a GeneJet PCR purification kit (Thermo) and eluted in 50 μ L of elution buffer. Thirty microliters of the eluted material was digested with 20 units of AarI enzyme and 25 units of Uracil-DNA Glycosylase in the NEB Cutsmart buffer in a 50 μ l final reaction volume for 2 h at 37 °C. The reaction was then purified using Dynabeads MyOne Streptavidin T1 beads (Life Technologies no. 65601) using the manufacturer's instructions. The nonbiotinylated strand was removed by washing the DNA coated Dynabeads in 50 μ L 1× SSC. Beads were then resuspended in 20 μ L of freshly prepared 0.15 M NaOH and incubated at room temperature for 10 min. Beads were then magnetized for 2 min and the supernatant was transferred to a new tube. The supernatant

contained the nonbiotinylated DNA strand. The probe was neutralized by adding 2.2 μL of 10× TE, pH 7.5 and 1.3 μL 1.25 M acetic acid. Dynabeads coated with biotinylated strands were washed once with 50 μL 0.1 M NaOH, once with 50 μL of B&W buffer, and once with 50 μL of TE buffer. The Dynabead solution was then heated to 95 °C for 10 min to cleave the apurinic sites and release the target staple sequence into solution. After magnetizing, the supernatant containing the target staple sequences was transferred to a new tub and repurified with a second round of Dynabead exposure.

Origami Designs. All notched rectangles (NR) were designed using CaDNAno software on the square lattice. ³⁰ The 7k-NRs were designed to be scaled-down versions of 51k-NRs. From crystallographic data, the rise per basepair of a DNA double-helix is $0.332 \pm (0.019 \text{ s.d.})$ nm. ⁴³ The effective diameter of helices packed in a square lattice is $2.6 \pm (0.1 \text{ s.d.})$ nm, as estimated from cryo-EM images of origami. ⁴⁴ These values were used to estimate each structures' dimensions, as shown in Supporting Information Table S2. CaDNAno design files and staple sequences are given in Supporting Information Note 6.

Origami Formation. Samples (between 30 and 100 μ L) were prepared by mixing the scaffold strand (between 5 and 0.5 nM) with the respective staple pool (in a 10× molar excess as compared to scaffold concentration) in the presence of 1× TAE/Mg²+ (40 mM Tris-HCl (pH 8.0), 20 mM acetic acid, 2 mM EDTA, and 12.5 mM magnesium acetate). Thermal anneals consisted of heating to 65 °C at the instrument's maximum rate, holding for 3 min, cooling to 20 °C over 1–8 h, and a quick drop to 4 °C in a Techne TC-3000 Thermal Cycler. All samples were held at 4 °C for at least 2 h prior to AFM imaging.

AFM Imaging. AFM imaging was performed on either a Digital Instruments Nanoscope IIIa with a multimode fluid-cell scanner head or an Asylum Research Cypher S with a droplet cantilever holder kit. Samples were prepared by pipetting 5 μ L of annealed origami onto freshly cleaved mica. Origami was allowed to incubate on mica for 3 min before applying 60 μ L of 1× TAE/Mg²⁺ for tapping mode AFM under buffer. Silicon nitride AFM tips from Veeco Inc. (DNP-10 or DNP-s10) were used for scans on the Nanoscope while silicon nitride AFM tips from Olympus (BioLever Mini) were used on the Cypher.

ASSOCIATED CONTENT

S Supporting Information

Details on the preparation and characterization of the $\lambda/M13$ hybrid scaffold (Table S1 and Figure S1), chip development (Figure S2), staple strand synthesis and amplification (Figures S3 and S4), origami designs (Table S2), AFM images of structures (Figures S5, S6, S7, and S8), CaDNAno.json files for DNA origami designs, $\lambda/M13$ hybrid scaffold sequence, and a list of the staple strand sequences employed for the origami structures. This material is available free of charge via the Internet at http://pubs.acs.org.

AUTHOR INFORMATION

Corresponding Author

*E-mail: thlabean@ncsu.edu.

Present Address

Gen9, 500 Technology Square, Cambridge, Massachusetts 02139, United States.

Author Contributions

The manuscript was written through contributions of all authors. All authors have given approval to the final version of the manuscript.

A.N.M. and I.S. contributed equally.

Notes

The authors declare no competing financial interest.

ACKNOWLEDGMENTS

The authors would like to thank S. Douglas (University of California at Santa Barbara) for providing a modified version of CaDNAno that would accommodate our large scaffold length. We would also like to thank B. Hove-Jensen (University of Copenhagen) and A. Rangnekar (North Carolina State University) for helpful discussions. This work has been funded by the National Science Foundation Grants CDI-0835794, OISE-1246799, and EPMD-1231888 and by the MolPhysX program at the University of Copenhagen.

REFERENCES

- (1) Whitesides, G. M.; Grzybowski, B. Science 2002, 295 (5564), 2418-2421.
- (2) Rothemund, P. W. K. Nature 2006, 440 (7082), 297-302.
- (3) Sharma, J.; Chhabra, R.; Andersen, C. S.; Gothelf, K. V.; Yan, H.; Liu, Y. J. Am. Chem. Soc. 2008, 130 (25), 7820-7821.
- (4) Kuzyk, A.; Laitinen, K. T.; Törmä, P. Nanotechnology 2009, 20 (23), 235305.
- (5) Maune, H. T.; Han, S.-p.; Barish, R. D.; Bockrath, M.; Iii, W. A. G.; Rothemund, P. W. K.; Winfree, E. *Nat. Nanotechnol.* **2010**, *5* (1), 61–66.
- (6) Gu, H.; Chao, J.; Xiao, S.-J.; Seeman, N. C. Nature **2010**, 465 (7295), 202–205.
- (7) Stephanopoulos, N.; Liu, M.; Tong, G. J.; Li, Z.; Liu, Y.; Yan, H.; Francis, M. B. *Nano Lett.* **2010**, *10* (7), 2714–2720.
- (8) Bui, H.; Onodera, C.; Kidwell, C.; Tan, Y.; Graugnard, E.; Kuang, W.; Lee, J.; Knowlton, W. B.; Yurke, B.; Hughes, W. L. *Nano Lett.* **2010**, *10* (9), 3367–3372.
- (9) Helmig, S.; Rotaru, A.; Arian, D.; Kovbasyuk, L.; Arnbjerg, J.; Ogilby, P. R.; Kjems, J.; Mokhir, A.; Besenbacher, F.; Gothelf, K. V. *ACS Nano* **2010**, *4* (12), 7475–7480.
- (10) Stein, I. H.; Schüller, V.; Böhm, P.; Tinnefeld, P.; Liedl, T. ChemPhysChem **2011**, 12 (3), 689–695.
- (11) Pilo-Pais, M.; Goldberg, S.; Samano, E.; LaBean, T. H.; Finkelstein, G. Nano Lett. **2011**, 11 (8), 3489—3492.
- (12) Lin, C.; Jungmann, R.; Leifer, A. M.; Li, C.; Levner, D.; Church, G. M.; Shih, W. M.; Yin, P. *Nat. Chem.* **2012**, *4* (10), 832–839.
- (13) Acuna, G. P.; Bucher, M.; Stein, I. H.; Steinhauer, C.; Kuzyk, A.; Holzmeister, P.; Schreiber, R.; Moroz, A.; Stefani, F. D.; Liedl, T.; Simmel, F. C.; Tinnefeld, P. ACS Nano 2012, 6 (4), 3189–3195.
- (14) Endo, M.; Sugita, T.; Katsuda, Y.; Hidaka, K.; Sugiyama, H. Chem.–Eur. J. 2010, 16 (18), 5362–5368.
- (15) Zhao, Z.; Yan, H.; Liu, Y. Angew. Chem., Int. Ed. **2010**, 49 (8), 1414–1417.
- (16) Woo, S.; Rothemund, P. W. K. Nat. Chem. 2011, 3 (8), 620-627.
- (17) Rajendran, A.; Endo, M.; Katsuda, Y.; Hidaka, K.; Sugiyama, H. ACS Nano **2011**, 5 (1), 665–671.
- (18) Endo, M.; Sugita, T.; Rajendran, A.; Katsuda, Y.; Emura, T.; Hidaka, K.; Sugiyama, H. *Chem. Commun.* **2011**, 47 (11), 3213–3215.
- (19) Rajendran, A.; Endo, M.; Hidaka, K.; Sugiyama, H. Chem. Commun. 2012, 49 (7), 686–688.
- (20) Hogberg, B. r.; Liedl, T.; Shih, W. M. J. Am. Chem. Soc. 2009, 131 (26), 9154–9155.
- (21) Marchi, A. N.; Saaem, I.; Tian, J.; LaBean, T. H. ACS Nano 2013, 7 (2), 903-910.
- (22) Yang, Y.; Han, D.; Nangreave, J.; Liu, Y.; Yan, H. ACS Nano 2012, 6 (9), 8209–8215.
- (23) Zhang, H.; Chao, J.; Pan, D.; Liu, H.; Huang, Q.; Fan, C. Chem. Commun. 2012, 48 (51), 6405–6407.

- (24) Devor, E.; Behlke, M. A. Integr. DNA Technol. 2005, 1-11.
- (25) Quan, J. Y.; Saaem, I.; Tang, N.; Ma, S. M.; Negre, N.; Gong, H.; White, K. P.; Tian, J. D. Nat. Biotechnol. 2011, 29 (5), 449–U239.
- (26) Dietz, H.; Douglas, S. M.; Shih, W. M. Science 2009, 325 (5941), 725-730.
- (27) Mathew-Fenn, R. S.; Das, R.; Harbury, P. A. B. Science **2008**, 322 (5900), 446–449.
- (28) Andersen, E. S. New Biotechnology 2010, 27 (3), 184–193.
- (29) Andersen, E. S.; Dong, M.; Nielsen, M. M.; Jahn, K.; Lind-Thomsen, A.; Mamdouh, W.; Gothelf, K. V.; Besenbacher, F.; Kjems, J. ACS Nano 2008, 2 (6), 1213–1218.
- (30) Douglas, S. M.; Marblestone, A. H.; Teerapittayanon, S.; Vazquez, A.; Church, G. M.; Shih, W. M. *Nucleic Acids Res.* **2009**, 37 (15), 5001–5006.
- (31) Kim, D.-N.; Kilchherr, F.; Dietz, H.; Bathe, M. *Nucleic Acids Res.* **2012**, 40 (7), 2862–2868.
- (32) Nickels, P. C.; Ke, Y.; Jungmann, R.; Smith, D. M.; Leichsenring, M.; Shih, W. M.; Liedl, T.; Högberg, B. *Small* **2014**, *10* (9), 1765–1769.
- (33) Sobczak, J.-P. J.; Martin, T. G.; Gerling, T.; Dietz, H. Science 2012, 338 (6113), 1458–1461.
- (34) Lin, C.; Perrault, S. D.; Kwak, M.; Graf, F.; Shih, W. M. Nucleic Acids Res. 2013, 41 (2), 40.
- (35) Bai, X.-c.; Martin, T. G.; Scheres, S. H. W.; Dietz, H. Proc. Natl. Acad. Sci. U.S.A. 2012, 109 (49), 20012–20017.
- (36) Vieira, J.; Messing, J. Production of single-stranded plasmid DNA. In *Methods in Enzymology*; Ray Wu, L. G., Ed.; Academic Press: New York, 1987; Vol. 153, pp 3–11.
- (37) Yamamoto, K. R.; Alberts, B. M.; Benzinger, R.; Lawhorne, L.; Treiber, G. Virology 1970, 40 (3), 734–744.
 - (38) Hove-Jensen, B. J. Microbiol. Methods 2008, 72 (2), 208-213.
- (39) Thon, G.; Bjerling, K. P.; Nielsen, I. S. Genetics 1999, 151 (3), 945–963.
- (40) Chang, A. C.; Cohen, S. N. J. Bacteriol. 1978, 134 (3), 1141-1156.
- (41) Saaem, I.; Ma, K.-S.; Marchi, A. N.; LaBean, T. H.; Tian, J. ACS Appl. Mater. Interfaces 2010, 2 (2), 491–497.
- (42) Quan, J.; Saaem, I.; Tang, N.; Ma, S.; Negre, N.; Gong, H.; White, K. P.; Tian, J. Nat. Biotechnol. 2011, 29 (5), 449–452.
- (43) Olson, W. K.; Gorin, A. A.; Lu, X.-J.; Hock, L. M.; Zhurkin, V. B. *Proc. Natl. Acad. Sci. U.S.A.* **1998**, 95 (19), 11163–11168.
- (44) Ke, Y.; Douglas, S. M.; Liu, M.; Sharma, J.; Cheng, A.; Leung, A.; Liu, Y.; Shih, W. M.; Yan, H. *J. Am. Chem. Soc.* **2009**, *131* (43), 15903–15908.